Eur Radiol (2007) 17: 2908–2920
DOI 10.1007/s00330-007-0680-4

NEURO

Fabrice Bonneville
Julien Savatovsky
Jacques Chiras

Imaging of cerebellopontine angle lesions: an update. Part 2: intra-axial lesions, skull base lesions that may invade the CPA region, and non-enhancing extra-axial lesions

Received: 25 December 2006
Revised: 11 March 2007
Accepted: 27 April 2007
Published online: 14 June 2007

F. Bonneville (✉) · J. Chiras
Department of Neuroradiology,
Pitié-Salpêtrière Hospital,
47, Boulevard de l'Hôpital,
75013 Paris, France
e-mail: fabrice.bonneville@psl.aphp.fr
Tel.: +33-142163596
Fax: +33-142163515

J. Savatovsky
Department of Radiology,
Adolphe de Rothschild Foundation,
Paris, France

Abstract Computed tomography (CT) and magnetic resonance (MR) imaging reliably demonstrate typical features of vestibular schwannomas or meningiomas in the vast majority of mass lesions responsible for cerebellopontine angle (CPA) syndrome. However, a large variety of unusual lesions can also be encountered in the CPA. Covering the entire spectrum of lesions potentially found in the CPA, these articles explain the pertinent neuroimaging features that radiologists need to know to make clinically relevant diagnoses in these cases, including data from diffusion- and perfusion-weighted imaging or MR spectroscopy, when available. A diagnostic algorithm based on the lesion's site of origin, shape and margins, density, signal intensity and contrast material uptake is also proposed. Non-enhancing extra-axial CPA masses are cystic (epidermoid cyst, arachnoid cyst, neurenteric cyst) or contain fat (dermoid cyst, lipoma). Tumours can also extend into the CPA by extension from the skull base (paraganglioma, chondromatous tumours, chordoma, cholesterol granuloma, endolymphatic sac tumour). Finally, brain stem or ventricular tumours can present with a significant exophytic component in the CPA that may be difficult to differentiate from an extra-axial lesion (lymphoma, hemangioblastoma, choroid plexus papilloma, ependymoma, glioma, medulloblastoma, dysembryoplastic neuroepithelial tumour).

Keywords Cerebellopontine angle · Brain tumours · Magnetic resonance imaging (MRI) · Diffusion-weighted MR imaging (DWI) · MR perfusion

Introduction

Although vestibular schwannomas and meningiomas represent the vast majority of mass lesions in the cerebellopontine angle (CPA), a large variety of unusual lesions can also be encountered in the CPA. In part 1, we initiated the diagnosis approach in front of a CPA lesion by reviewing the different enhancing extra-axial lesions arising directly from the CPA cistern and its content. In this paper, we continue with exophytic intra-axial lesions and skull base lesions which may invade the CPA, and also describe non-enhancing extra-axial lesions. A concise algorithm is proposed to facilitate diagnosis (Fig. 1).

Enhancing lesions

Extra-axial lesions originating in the CPA

Extra-axial lesions are theoretically easily recognized in the CPA. They are separated from the brain parenchyma by a cleft of cerebrospinal fluid and may enlarge the cerebellopontine cistern. They also push the cranial nerves, the brain stem or the anterior aspect of the cerebellum away. Demonstration of vessels interposed between the mass lesion and the brain parenchyma is another sign of the extra-axial origin of the lesion. Such lesions mainly include schwannomas and a wide spectrum of meningeal mass lesions described in detail in part 1.

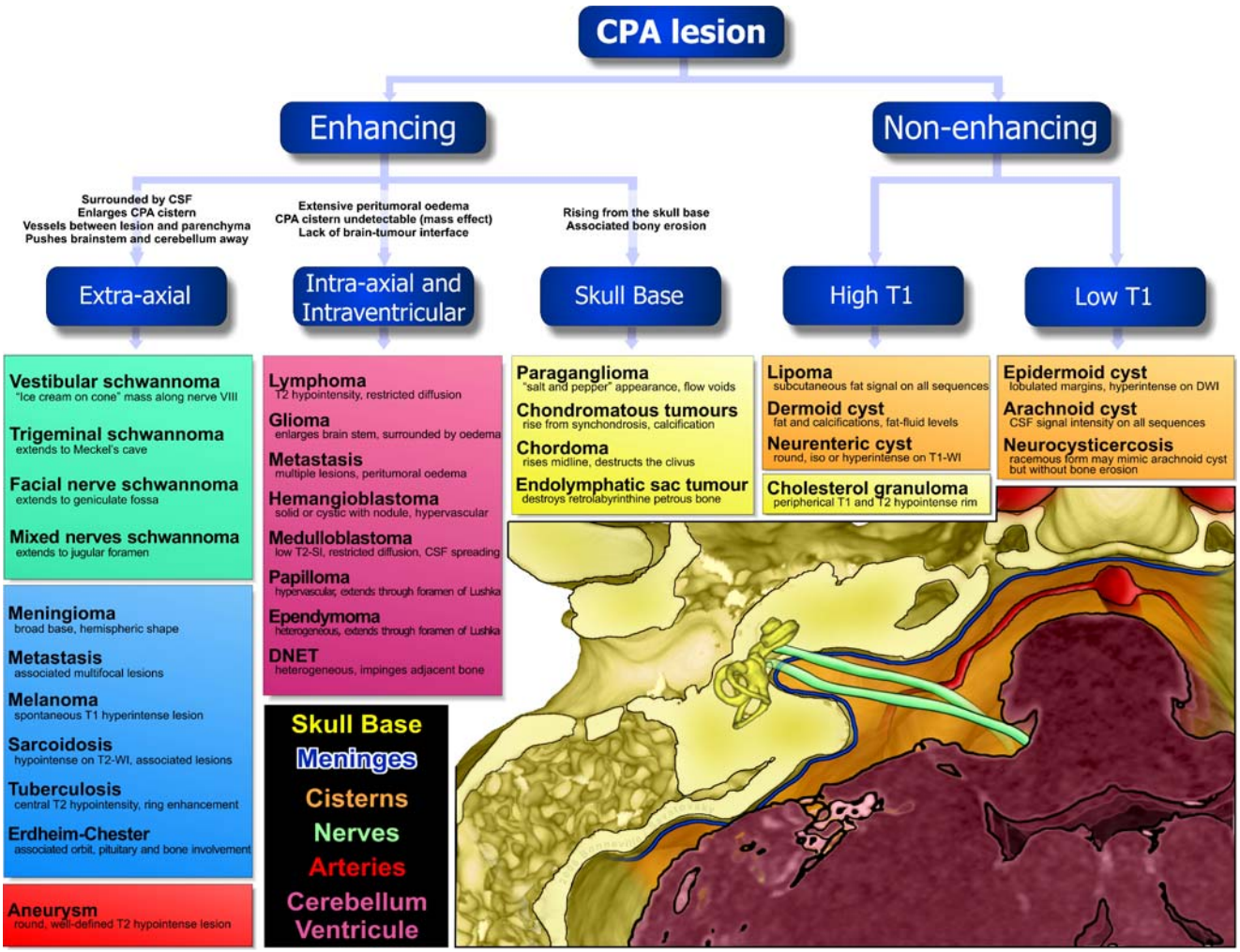

Fig. 1 Drawing of a segmental approach to diagnosis of CPA lesions based on gadolinium enhancement, site of origin and key feature

Intra-axial and intraventricular lesions

At imaging, precise anatomic landmarks are not always reliably depicted in the posterior fossa, and the intra- or extra-axial location of a lesion is not always certain, especially when the cistern itself is no longer depicted. Extensive peritumoral oedema surrounding an enhancing lesion, centred on a significant mass effect obliterating the CPA cistern is very unlikely in a benign extra-axial tumour. In this circumstance, an intra-axial tumour such as a lymphoma, a glioma or a metastasis should be suspected. The lack of clear brain-tumour interface may also favour an intra-axial origin.

Lymphoma

Primary central nervous system lymphomas may be either intra- or extra-axial in the CPA [1–3]. However, and except for the signs related to the location, imaging features are identical for both sites of origin. In immunocompetent patients, lymphomas appear with intermediate or hyperattenuation on CT with a uniform enhancement after contrast administration. At MRI, they appear with an intermediate to low signal intensity on T1-weighted images that strongly and homogeneously enhances after gadolinium administration, and a characteristic T2 low signal intensity in about 75% of the cases. This latter low signal intensity is due to the high cellularity of this tumour, which also explains the high signal intensity of lymphomas usually observed on diffusion-weighted imaging (DWI) with low apparent diffusion coefficient (ADC) values (Fig. 2) [4]. Because of the lack of neoangiogenesis and the increased permeability of the blood-brain barrier observed in lymphomas, these tumours present with rather low relative cerebral blood volume (rCBV) compared to other malignant intra-axial tumours. Indeed, their rCBV ratios are statistically lower (around 1) than those of metastases or high grade gliomas (around 5), thus providing a valuable criterion that allows differentiation among these lesions [5].

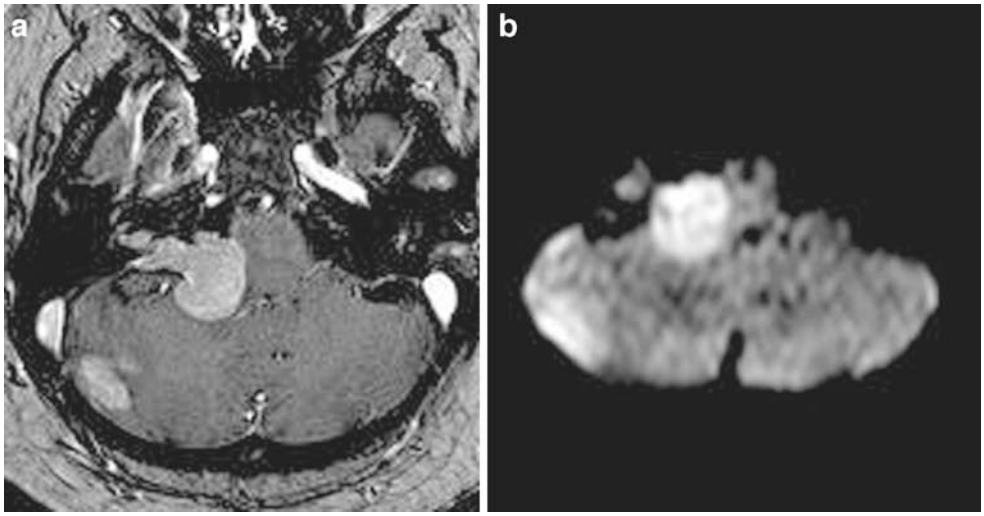

Fig. 2a, b Primary brain lymphoma in a 49-year-old man. **a** The axial gadolinium-enhanced T1-weighted MR image reveals an homogeneously enhanced right CPA lesion with intracanalicular portion that could mimic a vestibular schwannoma. **b** On diffusion-weighted image, the tumour appears with a high signal intensity and has restricted diffusion with a low apparent diffusion coefficient (not shown), a feature suggestive of lymphoma. Note the right cerebellar lesion also visible on **a** (courtesy of F. Cotton, MD, with permission from reference [4])

In immunocompromised individuals, lymphomas present usually as multiple peripherally enhancing lesions with marked peritumoral oedema [6]. However, due to the significant overlap in findings, lymphomas cannot always be reliably distinguished from toxoplasmosis, the main differential diagnosis in this situation, based on imaging findings on conventional sequences, as well as on DWI or perfusion MR [7].

Glioma

Glial tumours of the brain stem, and especially pilocytic astrocytomas in young adults, can manifest as asymmetric expansion of the brain stem that can rarely be pedunculated and exophytic, invading the CPA (Fig. 3) [3, 8] and even mimicking a vestibular schwannoma by enlarging the porus acusticus [9]. These tumours do not have specific imaging features in this location: they appear with T2 hyperintensity, T1 hypointensity and variable enhancement depending on the glioma grade. They are usually surrounded by adjacent oedema. Diffusion and perfusion imaging of the solid portions of glial tumours also depend on their histological grade. In general, the lower the ADC value, the higher the rCBV, the higher the grade [10].

Metastasis

Intracranial metastases are ubiquitous. They may be extra-axial and mimic a meningioma or a schwannoma in the CPA, as previously described in detail in the first part of this review, or be intra-axial, exactly located in front of the IAC, often surrounded by peritumoral oedema (Fig. 4). Multiple lesions or past history of a known cancer will lead to the diagnosis. Additionally, advanced MR techniques are helpful and demonstrate mean rCBV ratios lower than high grade gliomas, and higher ADC values than the enhancing portion of high grade gliomas and abscesses [11, 12]. MR spectroscopy shows a predominant peak in lipids in metastasis, another important finding considered suggestive of the diagnosis [13].

Hemangioblastoma

Hemangioblastomas are benign vascular intra-axial tumours preferentially located in the cerebellar hemispheres, with a possible extent into the CPA [3, 14]. They are sporadic in the vast majority of cases but are a manifestation of von Hipple-Lindau disease in 25%. This disorder is an autosomal-dominant phacomatosis leading to multiple retinal and cerebral hemangioblastomas, renal cell carcinomas and pancreatic cysts and tumours. Hemangioblastomas usually present as well-circumscribed masses with smooth margins, either entirely solid (40%) or cystic, with a hypervascular enhancing mural nodule (60%), around which oedema is usually absent. When cystic, the liquid component usually appears hypointense on T1-weighted images and hyperintense on T2-weighted images but slightly different than the CSF on fluid-attenuated inversion-recovery (FLAIR) sequence. The nodule is isodense on CT, isointense on both T1- and T2-weighted images, and enhances strongly and homogeneously after contrast media injection. Interestingly, the solid portions give low signal on DWI with increased ADC values, a finding usually not found in other cerebellar solid tumours. This finding may be explained by the rich vascular spaces present within hemangioblastomas [15]. Indeed, prominent flow voids in and/or around the solid portion of these hypervascular tumours are observed in some cases and are suggestive of the diagnosis. Perfusion MR imaging also

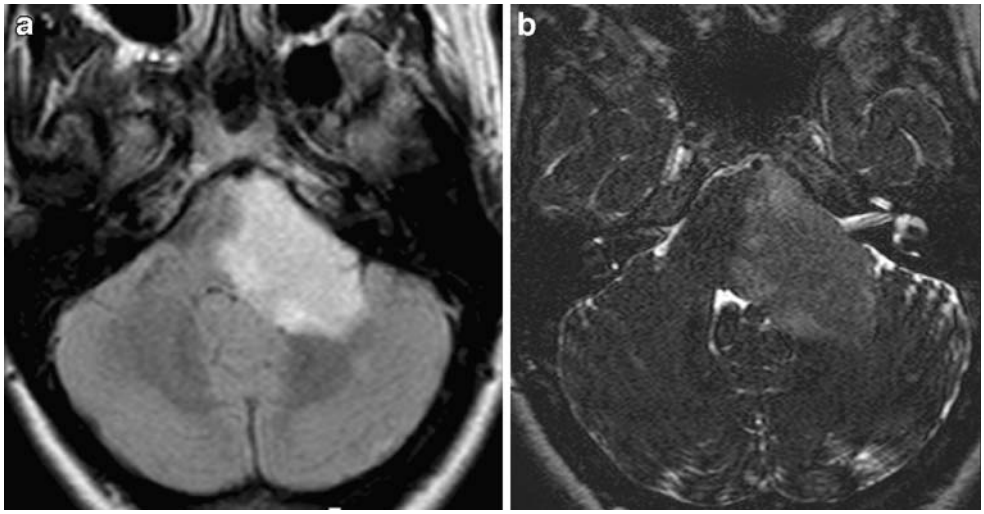

Fig. 3a, b Brain stem glioma in a 33-year-old woman with progressive left facial palsy, sensorineural hearing loss and dizziness. **a** Axial proton density-weighted image shows a high signal intensity lesion in the left CPA. **b** The axial infra-millimetric heavily T2-weighted image demonstrates the intra-axial location of the tumour with a faint tumour-parenchyma interface and the absence of intracanalicular component

reveals high rCBV ratios in these lesions (around 11), values significantly higher than those of metastases (around 5) [5]. The extensive hypervascular nature is also confirmed by cerebral angiography that shows dilated feeding arteries and a prolonged tumoral blush corresponding to the solid portion. Supraselective catheterization of the feeding vessels allows preoperative embolization of the tumour and can potentially decrease the morbidity and mortality of surgical resection [16].

Medulloblastoma

Medulloblastomas are primary neuroepithelial tumours that mainly occur midline in the posterior fossa of children. Differences in the imaging characteristics of adult medulloblastomas have been reported, including involvement of lateral cerebellar hemispheres with a possible extra-axial appearance [17], or even a primary extra-axial location mimicking either a meningioma [18, 19] or a vestibular schwannoma due to an extent into the internal auditory canal [20]. Medulloblastomas are highly cellular and consequently appear homogeneously isodense on CT, isointense or hypointense on T1- and T2-weighted images and enhance moderately after contrast administration. Irregularities at the brain-tumour interface may be a valuable clue to the intra-axial origin and therefore the diagnosis. CSF seeding frequently occurs with these particularly aggressive tumours, and should be sought with MR along the entire neuraxis before beginning the treatment. Presumably due to their high cellularity and high nuclear-to-cytoplasmic ratio, medulloblastomas show high signal intensity on DWI and have low ADCs [21]. At proton MR spectroscopy, medulloblastomas characteristically seem to show taurine, detectable at short echo time, and a massive choline peak [22].

Papilloma

Most papillomas in adults are located in the posterior fossa. Although they commonly arise from the fourth ventricle,

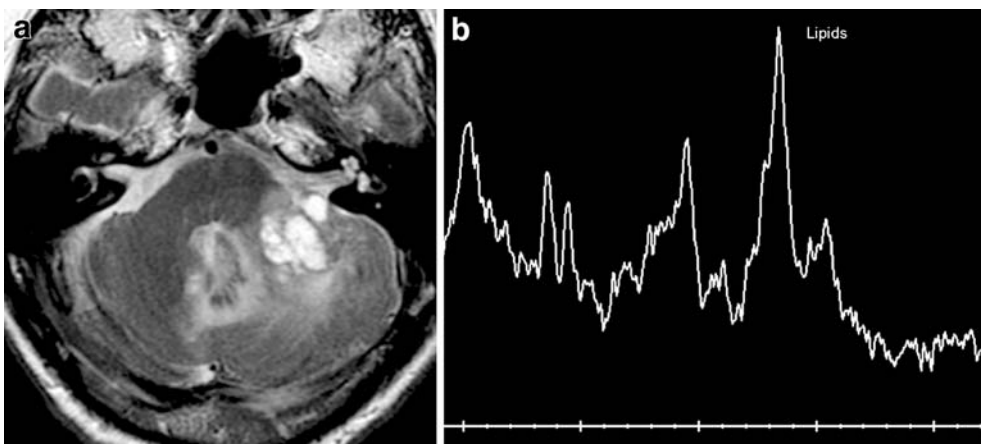

Fig. 4a, b Metastasis from a colon cancer in a 56-year-old man with dizziness and headache. **a** Axial T2-weighted image demonstrates a hyperintense cystic lesion in front of the left IAC. Peritumoral oedema and lack of CPA cistern widening are more in favour of an intra-axial lesion than a schwannoma. **b** Short TE MR spectroscopy reveals a predominant peak in lipids, a feature suggestive of metastasis

they occasionally extend into the CPA through the foramen of Lushka [23] or primarily occur there [3, 24]. Choroid plexus papillomas, which are benign, are structurally similar to normal choroid plexus and therefore appear as calcified, vascular, enhancing masses at CT, with possible intratumoral cyst [25]. At MRI, papillomas appear either as homogeneous or heterogeneous cauliflower-like tumours. They are mainly iso/hypointense on T1- and T2-weighted images and strongly enhance after contrast injection, unless the tumour is highly calcified. They may also contain areas of low signal intensity corresponding to calcifications, possible foci of high signal intensity due to intratumoral hemorrhage and flow voids when high flow vessels feed the tumour (Fig. 5) [26]. Cerebral digital subtraction angiograms reveal these enlarged arteries that demonstrate a prolonged vascular blush and intratumoral arteriovenous shunting, thus potentially mimicking an hemangioblastoma in this location [27]. Finally, hydrocephalus is often associated with choroid plexus papillomas; it may be explained in part by CSF hypersecretion by the tumour, but also by fourth ventricle obstruction when the tumour is located in the posterior fossa [28].

Ependymoma

Ependymomas are ubiquitous along the neuroaxis and may be either spinal, supratentorial or infratentorial, with a predilection for the fourth ventricle in the latter location [29]. More frequently than papillomas, ependymomas extend into the CPA by means of an exophytic component coming from the fourth ventricle through the foramen of Lushka, a pattern very suggestive of the diagnosis. Also, they arise directly within the CPA [30]. Ependymomas appear as irregular and lobulated isodense masses with common calcification at CT. At MRI, they appear heterogeneous with T1 hypointensity, T2 iso/hyperintensity and heterogeneous enhancement. They may demonstrate intratumoral microcysts, necrosis or hemorrhage [29]. Peritumoral oedema is usually absent.

Dysembryoplastic neuroepithelial tumour

Dysembryoplastic neuroepithelial tumours (DNT) have been described as clinicopathological neoplasms, usually located in the temporal lobe, associated with intractable complex partial seizure in young patients. Only rare cases have been reported in the posterior fossa [31, 32], including scattered reports in the CPA [3]. Diagnosis is based on the pathological analysis of the tumour but may be suggested in young adults who present with mild non-specific symptoms in association with a large heterogeneous lesion that may enhance. The mass may also impinge the adjacent bones if there is contact with the skull base [3]. No oedema has been reported in association with infratentorial DNTs.

Skull base lesions

A few tumours rising from the skull base may extend, partially or extensively, in the CPA. Significant bony erosion associated with the mass lesion points toward the diagnosis of this type of lesion.

Paraganglioma

Most paragangliomas located in the CPA result from the extension of paragangliomas arising at the jugular foramen (glomus jugulare tumour) or in the middle ear (glomus tympanicum tumour) [3]. Indeed, only three cases of primary paragangliomas originating from the CPA itself have been reported to date [33]. These benign but locally aggressive tumours destroy the bones of the skull base with a moth-eaten erosion pattern at CT. At MRI, paraganglio-

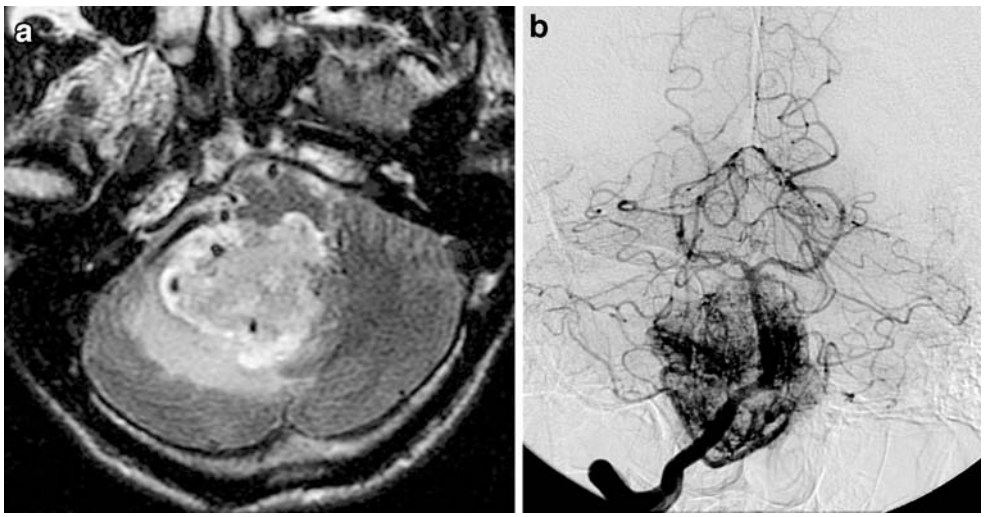

Fig. 5a, b Papilloma in a 28-year-old man with vertigo and intracranial hypertension syndrome. **a** Axial T2-weighted image reveals a large intraventricular lesion located at the bottom of the fourth ventricle extending in the right CPA through the right foramen of Lushka. The multiple flow voids observed in and around the lesion are in favour of a hypervascular lesion, as confirmed by **b**, a digital subtracted angiogram, with a feature suggestive of papilloma in this location

mas appear as highly vascular soft tissue lesions demonstrating a mix of multiple punctuate and serpentine signal voids corresponding to high-flow intratumoral vessels and foci of high-signal intensity due to intratumoral hemorrhages with methemoglobin, producing the characteristic salt-and-pepper appearance (Fig. 6) [34]. A combination of unenhanced and contrast-enhanced 3D time-of-flight MR angiography has been proposed in addition to a standard imaging protocol to increase the detection of these intratumoral vessels [35]. Perfusion MR imaging demonstrates high vascularity patterns with high rCBV. Finally conventional angiography demonstrates an intense tumoral blush with enlarged feeding arteries, which may allow haemostatic embolisation prior to surgical resection, though it is rarely used as a primary diagnostic modality [36].

Chondromatous tumours

Chondromas and chondrosarcomas develop from cartilaginous remnants enclosed in the synchondroses of the skull base. These tumours usually originate off midline, at the petro-occiptal fissure or near the jugular foramen, and they may subsequently extend into the CPA (Fig. 7) [37]. At CT, cartilaginous tumours are hypo- to isoattenuating, often contain calcifications and often destroy the adjacent bones. At MRI, the hyaline cartilaginous matrix of these tumours provides a low signal intensity on T1-weighted images and a very intense signal on T2-weighted images. The diagnosis is strongly suggested when this pattern is observed in a characteristic location. Frequently, areas of signal void consistent with calcifications are observed within the mass [38]. Chondromatous tumours usually enhance poorly due to their hypovascularity [39].

Chordoma

Intracranial chordomas are thought to originate from embryonic remnants of the primitive notochord and are located midline, near the clivus, from which they rarely extend into the CPA [3, 40]. Chondroid chordoma is a pathological subtype of chordoma that may have a more lateral origin in the petrous bone and grow directly in the CPA [41, 42]. All kinds of chordomas have, however, very similar imaging patterns, sometimes shared with chondrosarcomas as well, except that the latter usually have a more lateral origin [43]. At CT, intracranial chordoma typically appears as a centrally located, well-circumscribed, expansile soft-tissue mass associated with extensive lytic destruction of the clivus. At MRI, on T1-weighted MR images, chordomas demonstrate intermediate to low signal intensity, with foci of T1 signal hyperintensity that may represent either residual ossified fragments of the skull base, tumour calcification, collections of proteinaceous fluid or hemorrhage [40]. On T2-weighted MR images, they demonstrate very high signal intensity and septa of low signal intensity that are considered characteristic [44]. Slight enhancement is usually observed after contrast media administration.

Endolymphatic sac tumours

Endolymphatic sac tumours are aggressive papillary adenomatous tumours that originate from the endolymphatic sac, which is located at the posterior aspect of the petrous bone. These tumours may grow large enough to extend into the CPA and eventually compress the brain stem [45]. Endolymphatic sac tumours occur sporadically or in the

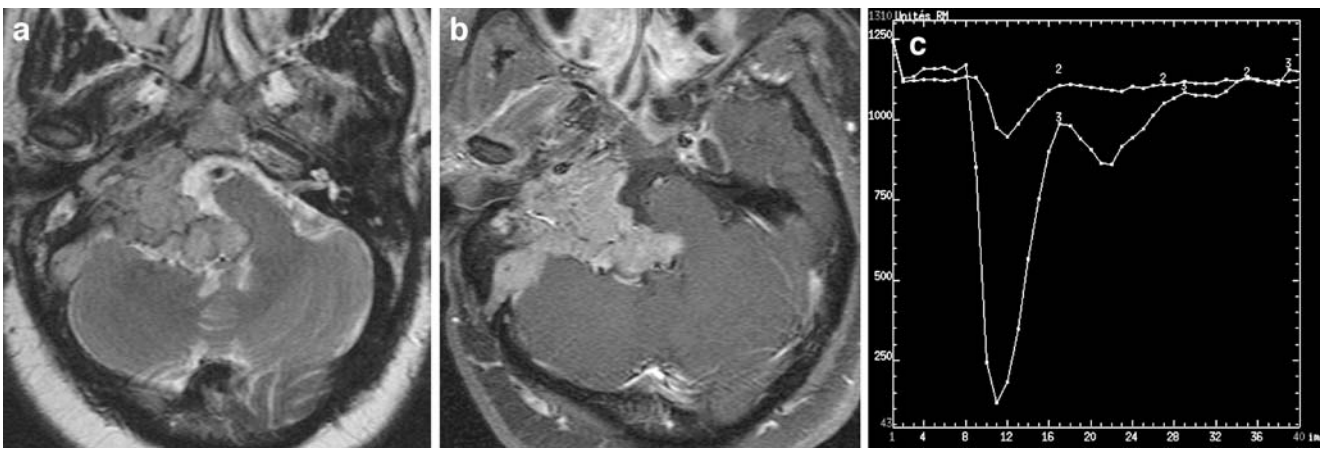

Fig. 6a–c Paraganglioma in a 36-year-old woman with right facial palsy, tinnitus, vertigo and sensorineural loss. **a** Axial T2-weighted image shows a voluminous hyperintense mass lesion widening the right CPA cistern, with multiple flow voids within and around the lesion. **b** Gadolinium-enhanced axial T1-weighted image with fat suppression better depicts the extent of the tumour in the skull base and the jugular foramen it comes from. **c** Perfusion imaging confirms the hyperperfusion of the tumour, as illustrated by the high relative cerebral blood volume observed on curve 3, compared to the normal curve 2

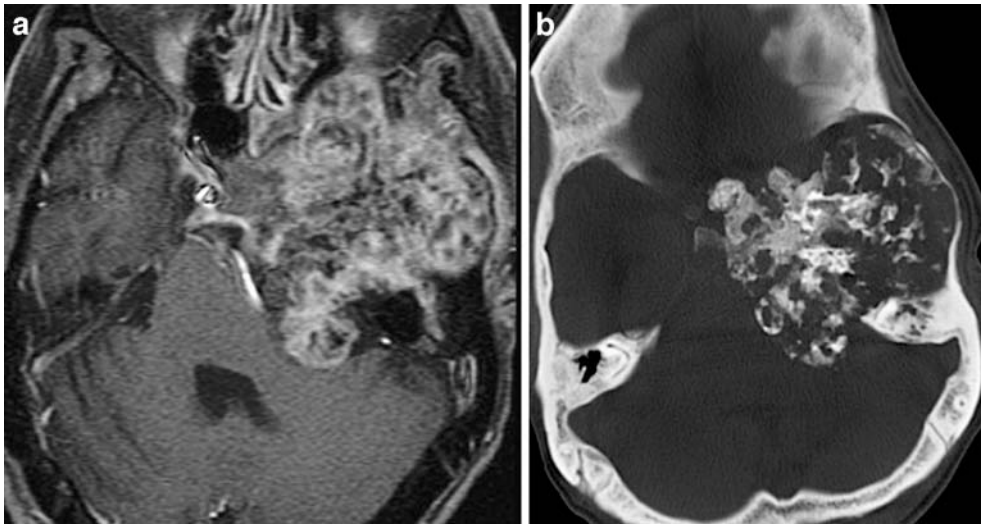

Fig. 7a, b Giant chondroma in a 33-year-old man with intracranial hypertension syndrome, right hemiparesia and aphasia. **a** Gadolinium-enhanced T1-weighted image with fat suppression demonstrates a large heterogeneous lesion of the skull base extending in the temporal fossa and the left CPA. **b** CT with bone algorithm better illustrates the massive intratumoral calcification, corresponding to the multiple foci of low signal intensity seen on **a**, and very suggestive of the chondromatous nature of the tumour

context of von Hipple-Lindau disease [46, 47]. Endolymphatic sac tumour is an extradural tumour that erodes and destroys the retrolabyrinthine petrous bone with geographic or moth-eaten margins at CT, and may exhibit possible calcifications [48]. At MRI, the lesion is heterogeneous on both T1- and T2-weighted images, with foci of high signal intensity due to intratumoral subacute hemorrhage. A T1- and T2-hyperintense cystic component, rich in blood and proteins, may be present and is suggestive of the diagnosis in this very specific location [3]. Notably, the cyst may be predominant and the mass itself can be almost completely cystic in appearance in some cases [46]. Finally, in masses larger than 2 cm in diameter, flow voids can be observed within and around these hypervascular tumours [48].

Non-enhancing lesions

T1 low-signal-intensity lesions

Epidermoid cyst

Epidermoid cysts are congenital lesions arising from the accidental inclusion of ectodermal epithelial tissue during neural tube closure in the first weeks of embryogenesis. About half of intracranial epidermoid cysts are located in the cerebellopontine angle, where they represent 5% of overall lesions and the third most common mass behind vestibular schwannomas and meningiomas [3]. Epidermoid cysts are lesions that grow from the slow desquamation of the stratified keratinised epithelium that lines the cyst. These malleable masses insinuate into posterior fossa cisterns, encasing cranial nerves and vessels with a specific irregular lobulated cauliflower-like outer surface [49]. Because of the relative softness of epidermoid cysts and their tendency to include rather than displace adjacent structures, clinical symptoms occur only when the masses are large. If epidermoid cysts commonly present with cranial nerve deficits and specifically trigeminal neuralgia [50], for which extension into Meckel's cave should be meticulously sought [51], brain stem stroke due to the stretching of basilar artery branches by the lesion is very unusual [52].

At CT, epidermoid cysts appear hypoattenuating with possible marginal calcifications. At MRI, they have a fluid-like low T1 signal intensity and high T2 signal intensity, but they are slightly brighter than CSF on both T1- and T2-weighted images. They may, however, be difficult to distinguish from arachnoid cysts on these sequences, based on signal intensity alone. With advances in MRI techniques, preoperative diagnosis of epidermoid cysts, and reliable distinction of these lesions from arachnoid cysts, should no longer pose a dilemma. On FLAIR sequence, epidermoid cysts can be easily differentiated from arachnoid cysts because the former show mixed iso- to hypersignal intensities, but with poor demarcation, while the signal of the latter is suppressed, like the signal of CSF (Fig. 8) [53]. MR cisternography, by means of heavily T2-weighted 3D sequence, demonstrates an epidermoid cyst signal hypointense to CSF, reveals the lobulated margins of the tumour, and clearly depicts the anatomical relation to neighbouring nerves and vessels and its precise extent for surgical planning [53, 54]. DWI offers a finding specific for extra-axial epidermoid cysts by showing a very high signal. Restricted ADC compared to CSF, almost comparable to that of the brain, and T2 shine-through effect both play an important role in the high signal intensity of epidermoid cyst at DWI [53, 55]. DWI is also crucial in the postoperative follow-up as it allows confirmation of the presence of a possible residual tumour [56]. Finally, MR spectroscopy is also helpful as it shows only elevated lactate peaks in these

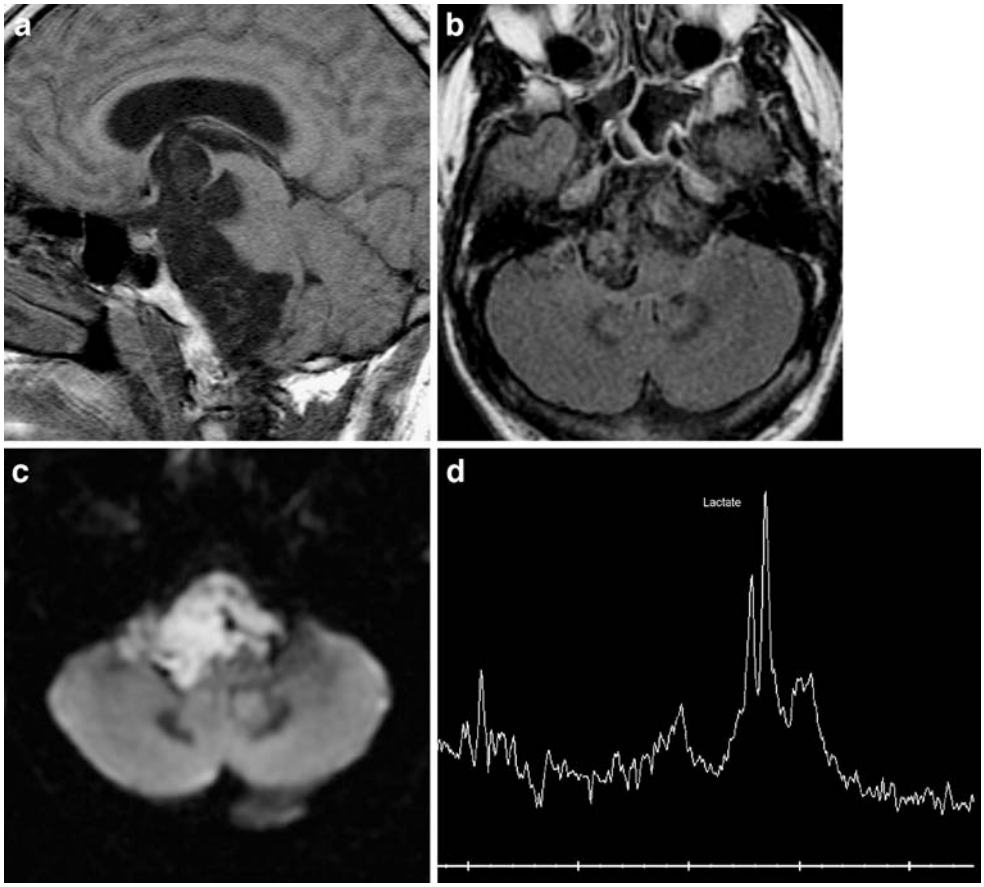

Fig. 8a–d Epidermoid cyst in a 24-year-old man with cranial nerves palsies. **a** Sagittal T1-weighted image reveals a voluminous hypointense extra-axial lesion indenting the brain stem. **b** On the axial FLAIR image, the tumour appears with an heterogeneous signal intensity, different from that of cerebrospinal fluid. **c** Diffusion-weighted image shows high signal intensity, a feature characteristic of an epidermoid tumour in this location. **d** MR spectroscopy demonstrates a predominant peak in lactate, another suggestive feature of epidermoid cyst

tumours [57], which can be of interest in case of atypical epidermoid cysts. Indeed, in very limited cases, unusual patterns of epidermoid cysts may be observed on MRI. Such circumstances include so-called white epidermoids which have a rich protein content and appear with reversed signal intensities with homogeneous high signal intensity on T1-weighted images and low signal intensity on T2-weighted images [58], intracystic hemorrhage with heterogeneous signal intensities due to blood products [59] or malignant transformation into squamous cell carcinoma which should be considered in case of frank contrast enhancement [60].

Arachnoid cyst

Arachnoid cysts are congenital, benign, intra-arachnoid pouch-like lesions filled with normal CSF. Their exact origin is uncertain, but they could result from a splitting of the embryonic meninges [49]. They are usually supratentorial, with about 70% being in the temporal fossa, mostly on the left side [61], anterior to the temporal poles. Only 10% of arachnoid cysts are located in the posterior fossa, where they most commonly develop in the CPA. The large majority of arachnoid cysts are asymptomatic and found incidentally at imaging, but they can compromise cranial nerve functions in the posterior fossa by stretching them. Spontaneous or traumatic intracystic hemorrhage can also complicate arachnoid cysts, though this has only rarely been described in the posterior fossa [62]. At neuroimaging, attenuation and signal intensities of uncomplicated arachnoid cysts exactly match those of CSF on all sequences, do not enhance after contrast media administration, and therefore, may mimic epidermoid cysts on conventional T1- and T2-weighted images. However, arachnoid cysts displace adjacent arteries and cranial nerves rather than encasing them, as epidermoid cysts usually do [3]. They also demonstrate rounded edges, smoothly deforming the adjacent brain or scalloping the bony structures. Additionally, the complete suppression of signal intensity on FLAIR sequence in arachnoid cysts and the lack of diffusion restriction of these lesions on DWI should eliminate epidermoid cyst as a likely differential diagnosis of arachnoid cysts (Fig. 9) [63].

Neurocysticercosis

Neurocysticercosis, a parasitosis due to *Taenia solium*, may present in its racemose form with multiple non-enhancing subarachnoid cysts, sometimes located in the CPA [64]. They appear as lobulated cysts with no mural nodule, no

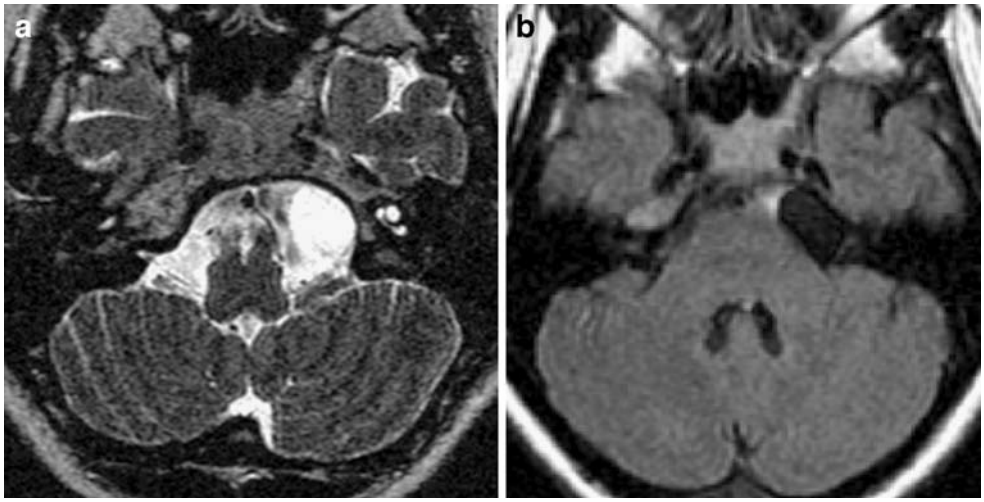

Fig. 9a, b Arachnoid cyst in a 16-year-old woman with headache. **a** The axial infra-millimetric heavily T2-weighted image reveals a well-demarcated round hyperintense lesion in the left CPA smoothly eroding the skull base. **b** On FLAIR sequence, the arachnoid cyst signal appears completely suppressed, even more than the free CSF that pulses in front of the brain stem

enhancement and have signal intensity similar to that of CSF, which makes arachnoid cyst the main differential diagnosis. The lack of bone erosion adjacent to the cyst is helpful in distinguishing these entities, and diagnosis of neurocysticercosis should then be considered in a patient from an endemic area [64, 65]. On DWI, neurocysticercosis cysts have hypointense signal with an apparent diffusion coefficient similar to that of CSF. DWI may fail to detect racemose lesions [66]. As an alternative, non-invasive MR cisternography by means of FLAIR sequence acquired after a 5-min inhalation of 100% O_2, which increases the signal of normal CSF, has been proposed as a robust technique to detect subarachnoid cysticercosis lesions [67].

T1 high-signal-intensity lesions

An intrinsic T1 high-signal intensity of a non-enhancing CPA mass lesion favours a fatty or high protein content. T1-weighted sequence with fat signal suppression should then be performed in order to distinguish the exact nature of the high signal intensity: if it is suppressed, the tumour contains fat and is likely to be a lipoma or a dermoid cyst, if it is unchanged, the lesion has a high protein content and may be a neurenteric cyst or a cholesterol granuloma.

Lipoma

Lipomas are benign lesions believed to result from a maldifferentiation of the primitive meninx. The majority of intracranial lipomas are located around the corpus callosum

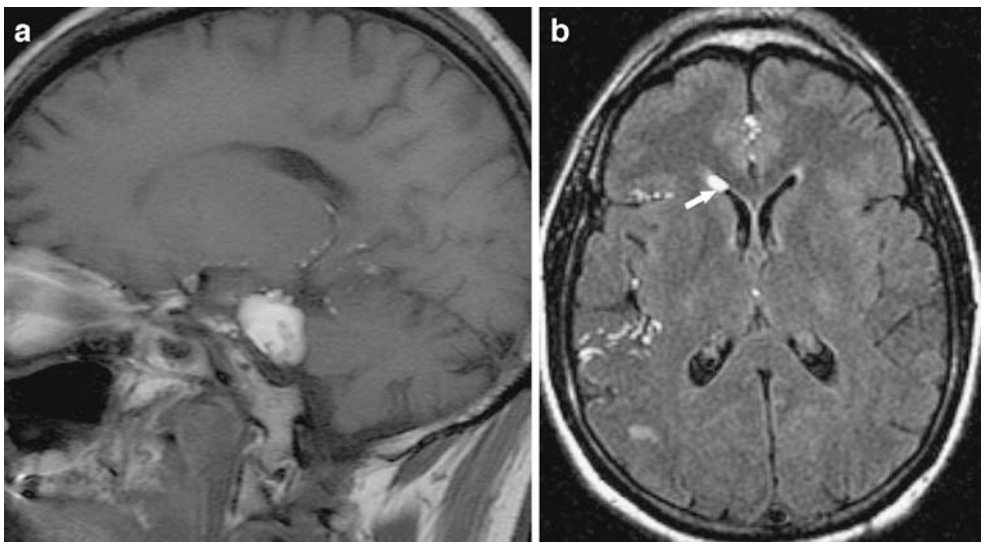

Fig. 10a, b Ruptured dermoid cyst in a 50-year-old man with sudden headache. **a** Sagittal T1-weighted image depicts a large heterogeneously hyperintense CPA lesion and multiple subtle subarachnoid foci of high signal intensity consistent with fat droplets. **b** Axial FLAIR image demonstrates multiple fatty droplets in the supratentorial sulci, as well as a fat-fluid level in the right frontal horn (*arrow*), a feature very suggestive of the diagnosis

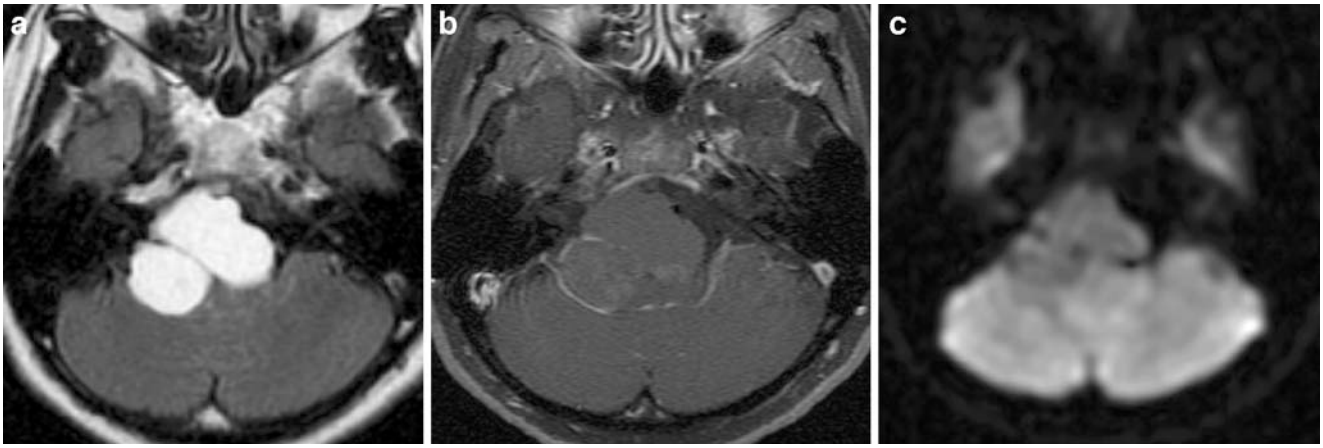

Fig. 11a–c Neurenteric cyst in 46-year-old man with cranial nerve palsies. **a** Axial FLAIR image reveals a cystic mass in the right CPA with smooth margins and an unusual homogeneous marked hyperintense signal. **b** Axial contrast-enhanced T1-weighted image with fat suppression only demonstrates a subtle peripheral linear discontinued enhancement at the posterior edge of this iso-signal-intensity lesion. **c** On diffusion-weighted image, the lesion does not show high signal intensity as epidermoid cysts do, but appears with isointensity, certainly because of a T2 shine-through effect and a high ADC (2,000 10-3 mm^2/s)

and about 100 cases have been reported in the CPA, where they encase normal adjacent neurovascular structures with very dense adhesions [68]. Intracranial lipomas may be asymptomatic, incidentally discovered on brain imaging. They can also produce symptoms by compressing the adjacent cerebral structures, such as the cranial nerves in the CPA [69]. At imaging, lipomas appear exactly the same as subcutaneous fat: homogeneously hypoattenuating on CT (except for possible superficial calcification) and with an homogeneous very high signal intensity on T1-weighted images, which decreases on fat-suppressed images, while no enhancement is observed after contrast administration [3].

Dermoid cyst

Dermoid cysts result from the congenital inclusion of cutaneous ectoderm. Intracranial dermoid cysts are intradural extra-axial lesions, predominantly supratentorial near midline [49]. Dermoid cysts are rare in the CPA, and may be secondary to the caudal extension of a parasellar lesion, the most frequent intracranial site of their occurrence [40]. They are heterogeneous masses containing a mix of fat, hair, calcifications and the products of sebaceous glands and desquamation of a keratinized epithelium. At imaging, a dermoid cyst appears as a well-circumscribed fatty round mass with a thick peripheral capsule that may enhance. In case of rupture, the visualisation of fatty T1-hyperintense droplets in the sulci or a fat-fluid level in the ventricles is highly suggestive of the diagnosis (Fig. 10).

Neurenteric cyst

Neurenteric cysts are congenital cystic masses lined by a mucin-producing epithelium of endodermal origin, closely

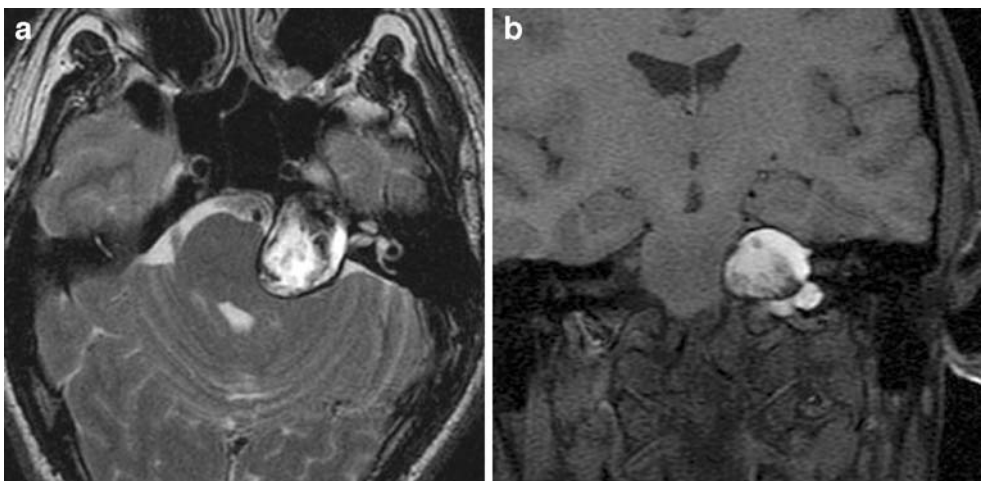

Fig. 12a, b Cholesterol granuloma in a 34-year-old man with left trigeminal neuralgia. **a** Axial T2-weighted image reveals a petrous apex lesion with a typical high-signal-intensity core surrounded by a hypointense rim which represents expanded cortical bone and hemosiderin peripheral deposits. **b** Coronal fat-suppressed T1-weighted image demonstrates the persistence of the central high signal intensity on this sequence, indicative of a high protein content rather than fat, a feature suggestive of a cholesterol granuloma in this specific location

resembling gastrointestinal tract mucosa. Neurenteric cysts adjacent to the central nervous system are mostly seen within the spinal canal, ventral to the spinal cord. Intracranial neurenteric cysts are very unusual, mainly located near the midline in the posterior fossa or in the CPA [70, 71]. They present with round and smooth margins. The signal intensity of the cyst depends on its protein content. It can rarely mimic CSF when this content is low [72], but it is often isointense to hyperintense relative to brain parenchyma on T1-weighted images and hyperintense on T2-weighted images when the protein concentration is high [49, 71]. Neurenteric cysts very rarely show peripheral rim enhancement [71]. Differences exist in reports of the signal intensity on DWI and ADC values of neurenteric cysts [71, 73]. However, based on the few cases of these cysts studied by DWI, it seems that the low signal intensity of neurenteric cysts on this sequence predominates (Fig. 11). This imaging feature may enable differentiation from epidermoid cysts, which may exhibit similar intensities on conventional sequences but a characteristic high signal intensity on DWI [73].

Cholesterol granuloma

Cholesterol granulomas result from the chronic obstruction of air cells and the subsequent accumulation of their secretions. In case of petrous apex origin, they can become large enough to expand in the CPA where they can compromise cranial nerves [74]. They appear as expansile lytic lesions of the temporal bone with sharp and smooth margins, demonstrating a central region of high signal intensity and a peripheral hypointense rim on both T1- and T2-weighted images, the latter corresponding to the association of the expanded cortical bone and hemosiderin deposits (Fig. 12) [3]. When desiccated, cholesterol granulomas can demonstrate areas of low signal intensity that give this homogeneous T1-hyperintense lesion an heterogeneous T2 pattern very suggestive of the diagnosis in this location [75]. Cholesterol granuloma could be classified as a skull base lesion invading the CPA, but the usual lack of enhancement after contrast enhancement and its characteristic intrinsic T1-high signal intensity, make its classification in this category more relevant.

Conclusion

A wide variety of lesions can be encountered in the CPA. A meticulous analysis of the site of origin, shape, density, signal intensities and behaviour after contrast media injection allows a systematic approach to the preoperative diagnosis in the majority of cases. Diffusion- and perfusion-weighted imaging, as well as MR spectroscopy may also provide crucial information that helps radiologists arrive at the correct diagnosis non-invasively.

Acknowledgements We are grateful to David Seidenwurm, MD, for his meticulous and exhaustive review of this manuscript.

References

1. Jaiswal AK, Mahapatra AK, Sharma MC (2004) Primary central nervous lymphoma presenting as bilateral cerebellopontine angle lesions: a rare case report. J Clin Neurosci 11:328–331
2. Danchaivijitr N, Hesselink JR, Aryan HE, Herndier B (2004) Cerebello-pontine angle (CPA) lymphoma with perineural extension into the middle fossa: case report. Surg Neurol 62:80–85
3. Bonneville F, Sarrazin JL, Marsot-Dupuch K et al (2001) Unusual lesions of the cerebellopontine angle: a segmental approach. Radiographics 21:419–438
4. Cotton F, Ongolo-Zogo P, Louis-Tisserand G et al (2006) Diffusion and perfusion MR imaging in cerebral lymphomas. J Neuroradiol 33:220–228
5. Hakyemez B, Erdogan C, Bolca N et al (2006) Evaluation of different cerebral mass lesions by perfusion-weighted MR imaging. J Magn Reson Imaging 24:817–824
6. Johnson BA, Fram EK, Johnson PC, Jacobowitz R (1997) The variable MR appearance of primary lymphoma of the central nervous system: comparison with histopathologic features. AJNR Am J Neuroradiol 18:563–572
7. Camacho DL, Smith JK, Castillo M (2003) Differentiation of toxoplasmosis and lymphoma in AIDS patients by using apparent diffusion coefficients. AJNR Am J Neuroradiol 24:633–637
8. Yousry I, Muacevic A, Olteanu-Nerbe V, Naidich TP, Yousry TA (2004) Exophytic pilocytic astrocytoma of the brain stem in an adult with encasement of the caudal cranial nerve complex (IX–XII): presurgical anatomical neuroimaging using MRI. Eur Radiol 14:1169–1173
9. Takada Y, Ohno K, Tamaki M, Hirakawa K (1999) Cerebellopontine angle pilocytic astrocytoma mimicking acoustic schwannoma. Neuroradiology 41:949–950
10. Fan GG, Deng QL, Wu ZH, Guo QY (2006) Usefulness of diffusion/perfusion-weighted MRI in patients with non-enhancing supratentorial brain gliomas: a valuable tool to predict tumour grading? Br J Radiol 79:652–658
11. Grand S, Kremer S, Tropres I et al (2006) Perfusion-diffusion 1H spectroscopy: role in the diagnosis and follow-up of supratentorial brain tumours in adults. Rev Neurol (Paris) 162:1204–1220

12. Krabbe K, Gideon P, Wagn P et al (1997) MR diffusion imaging of human intracranial tumours. Neuroradiology 39:483–489
13. Bulakbasi N, Kocaoglu M, Ors F, Tayfun C, Ucoz T (2003) Combination of single-voxel proton MR spectroscopy and apparent diffusion coefficient calculation in the evaluation of common brain tumors. AJNR Am J Neuroradiol 24:225–233
14. Dow GR, Sim DW, O'Sullivan MG (2002) Excision of large solid haemangioblastomas of the cerebellopontine angle by a skull base approach. Br J Neurosurg 16:168–171
15. Quadery FA, Okamoto K (2003) Diffusion-weighted MRI of haemangioblastomas and other cerebellar tumours. Neuroradiology 45:212–219
16. Abo-Al Hassan A, Ismail M, Panda SM (2006) Pre-operative endovascular embolization of a cerebellar haemangioblastoma. A case report. Med Princ Pract 15:459–462
17. Jaiswal AK, Mahapatra AK, Sharma MC (2004) Cerebellopontine angle medulloblastoma. J Clin Neurosci 11:42–45
18. Gil-Salu JL, Rodriguez-Pena F, Lopez-Escobar M, Palomo MJ (2004) Medulloblastoma presenting as an extra-axial tumor in the cerebellopontine angle. Neurocirugia (Astur) 15:285–289
19. Izycka-Swieszewska E, Debiec-Rychter M, Kloc W (2003) Primitive neuroectodermal tumor in the cerebellopontine angle with isochromosome 17q presenting as meningioma in a woman 26 years of age. Clin Neuropathol 22:66–70
20. Kalamarides M, Dewolf E, Couvelard A et al (2001) Extraaxial primitive neuroectodermal tumor mimicking a vestibular schwannoma: diagnostic and therapeutic difficulties. Report of two cases. J Neurosurg 94:612–616
21. Rodallec M, Colombat M, Krainik A et al (2004) Diffusion-weighted MR imaging and pathologic findings in adult cerebellar medulloblastoma. J Neuroradiol 31:234–237
22. Moreno-Torres A, Martinez-Perez I, Baquero M et al (2004) Taurine detection by proton magnetic resonance spectroscopy in medulloblastoma: contribution to noninvasive differential diagnosis with cerebellar astrocytoma. Neurosurgery 55:824–829; discussion 829
23. Beskonakli E, Cayli S, Bostanci U, Kulacoglu S, Yalcinlar Y (1998) Choroid plexus papillomas of the posterior fossa: extraventricular extension, intraventricular and primary extraventricular location. Report of four cases. J Neurosurg Sci 42:37–40
24. Mitsuyama T, Ide M, Hagiwara S et al (2005) Adult choroid plexus papilloma of the posterior fossa: extraventricular location. No Shinkei Geka 33:825829
25. Li S, Savolaine ER (1996) Imaging of atypical choroid plexus papillomas. Clin Imaging 20:85–90
26. Shin JH, Lee HK, Jeong AK et al (2001) Choroid plexus papilloma in the posterior cranial fossa: MR, CT, and angiographic findings. Clin Imaging 25:154–162
27. Garcia-Valtuille R, Abascal F, Garcia-Valtuille AI et al (2000) Adult choroid plexus papilloma of the posterior fossa mimicking a hemangioblastoma. Case report. J Neurosurg 92:870–872
28. Pencalet P, Sainte-Rose C, Lellouch-Tubiana A et al (1998) Papillomas and carcinomas of the choroid plexus in children. J Neurosurg 88:521–528
29. Choi JY, Chang KH, Yu IK et al (2002) Intracranial and spinal ependymomas: review of MR images in 61 patients. Korean J Radiol 3:219–228
30. Torun F, Tuna H, Bozkurt M, Deda H (2005) Extra-axial ependymoma of posterior fossa extending to the Meckel's cave. Clin Neurol Neurosurg 107:334–336
31. Litrico S, Desjardins T, Dran G, Michiels JF, Paquis P (2004) Infratentorial localisation of a dysembryoplastic neuroepithelial tumor. A case report. Neurochirurgie 50:47–52
32. Fujimoto K, Ohnishi H, Tsujimoto M, Hoshida T, Nakazato Y (2000) Dysembryoplastic neuroepithelial tumor of the cerebellum and brainstem. Case report. J Neurosurg 93:487–489
33. Deb P, Sharma MC, Gaikwad S et al (2005) Cerebellopontine angle paraganglioma — report of a case and review of literature. J Neurooncol 74:65–69
34. Lee KY, Oh YW, Noh HJ et al (2006) Extraadrenal paragangliomas of the body: imaging features. AJR Am J Roentgenol 187:492–504
35. van den Berg R, Verbist BM, Mertens BJ, van der Mey AG, van Buchem MA (2004) Head and neck paragangliomas: improved tumor detection using contrast-enhanced 3D time-of-flight MR angiography as compared with fat-suppressed MR imaging techniques. AJNR Am J Neuroradiol 25:863–870
36. van den Berg R (2005) Imaging and management of head and neck paragangliomas. Eur Radiol 15:1310–1318
37. Cummings TJ, Bridge JA, Fukushima T (2004) Extraskeletal myxoid chondrosarcoma of the jugular foramen. Clin Neuropathol 23:232–237
38. Bourgouin PM, Tampieri D, Robitaille Y et al (1992) Low-grade myxoid chondrosarcoma of the base of the skull: CT, MR, and histopathology. J Comput Assist Tomogr 16:268–273
39. Brownlee RD, Sevick RJ, Rewcastle NB, Tranmer BI (1997) Intracranial chondroma. AJNR Am J Neuroradiol 18:889–893
40. Bonneville F, Cattin F, Marsot-Dupuch K et al (2006) T1 signal hyperintensity in the sellar region: spectrum of findings. Radiographics 26:93–113
41. Takenaka K, Nishimura Y, Andoh T et al (1992) Delayed postcontrast CT and MR imaging of chondroid chordoma-case report. Neurol Med Chir (Tokyo) 32:28–31
42. Mohanty PP, Pasricha R, Datta NR, Jain M (2003) Primary chondroid chordoma of the petrous part of the temporal bone. Clin Oncol (R Coll Radiol) 15:365–366
43. Pamir MN, Ozduman K (2006) Analysis of radiological features relative to histopathology in 42 skull-base chordomas and chondrosarcomas. Eur J Radiol 58:461–470
44. Erdem E, Angtuaco EC, Van Hemert R, Park JS, Al-Mefty O (2003) Comprehensive review of intracranial chordoma. Radiographics 23:995–1009
45. Joseph BV, Chacko G, Raghuram L, Rajshekhar V (2002) Endolymphatic sac tumor: a rare cerebellopontine angle tumor. Neurol India 50:476–479
46. Kilickesmez O (2006) Endolymphatic sac tumor in a patient with von Hippel-Lindau disease: MR imaging findings. Diagn Interv Radiol 12:14–16
47. Muzumdar DP, Goel A, Fattepurkar S, Goel N (2006) Endolymphatic sac carcinoma of the right petrous bone in von Hippel-Lindau disease. J Clin Neurosci 13:471–474
48. Mukherji SK, Albernaz VS, Lo WW et al (1997) Papillary endolymphatic sac tumors: CT, MR imaging, and angiographic findings in 20 patients. Radiology 202:801–808
49. Osborn AG, Preece MT (2006) Intracranial cysts: radiologic-pathologic correlation and imaging approach. Radiology 239:650–664

50. Meng L, Yuguang L, Feng L et al (2005) Cerebellopontine angle epidermoids presenting with trigeminal neuralgia. J Clin Neurosci 12:784–786
51. Sarrazin JL (2006) Infra tentorial tumors. J Radiol 87:748–763
52. Yilmazlar S, Kocaeli H, Cordan T (2004) Brain stem stroke associated with epidermoid tumours: report of two cases. J Neurol Neurosurg Psychiatry 75:1340–1342
53. Liu P, Saida Y, Yoshioka H, Itai Y (2003) MR imaging of epidermoids at the cerebellopontine angle. Magn Reson Med Sci 2:109–115
54. Murakami N, Matsushima T, Kuba H et al (1999) Combining steady-state constructive interference and diffusion-weighted magnetic resonance imaging in the surgical treatment of epidermoid tumors. Neurosurg Rev 22:159–162
55. Annet L, Duprez T, Grandin C et al (2002) Apparent diffusion coefficient measurements within intracranial epidermoid cysts in six patients. Neuroradiology 44:326–328
56. Dechambre S, Duprez T, Lecouvet F, Raftopoulos C, Gosnard G (1999) Diffusion-weighted MRI postoperative assessment of an epidermoid tumour in the cerebellopontine angle. Neuroradiology 41:829–831
57. Nguyen JB, Ahktar N, Delgado PN, Lowe LH (2004) Magnetic resonance imaging and proton magnetic resonance spectroscopy of intracranial epidermoid tumors. Crit Rev Comput Tomogr 45:389–427
58. Bonneville F, Cattin F, Katranji H, Bonneville JF (2005) Clinical case #4. Atypical epidermoid cyst of the cerebellar vermis. J Radiol 86:523–526
59. Chen CY, Wong JS, Hsieh SC, Chu JS, Chan WP (2006) Intracranial epidermoid cyst with hemorrhage: MR imaging findings. AJNR Am J Neuroradiol 27:427–429
60. Tamura K, Aoyagi M, Wakimoto H et al (2006) Malignant transformation eight years after removal of a benign epidermoid cyst: a case report. J Neurooncol
61. Wester K, Svendsen F, Hugdahl K (1999) Intracranial arachnoidal cysts-localization, gender and sidedness. Tidsskr Nor Laegeforen 119:4162–4164
62. Ikeda H, Deinsberger W, Boker DK (2000) Petroclival arachnoid cyst presenting with spontaneous intracystic haemorrhage-case presentation. Acta Neurochir (Wien) 142:1317–1318
63. Dutt SN, Mirza S, Chavda SV, Irving RM (2002) Radiologic differentiation of intracranial epidermoids from arachnoid cysts. Otol Neurotol 23:84–92
64. Jarupant W, Sithinamsuwan P, Udommongkol C et al (2004) Spinal cord compression and bilateral sensory neural hearing loss: an unusual manifestation of neurocysticercosis. J Med Assoc Thai 87:1244–1249
65. Duchene M, Benoudiba F, Iffenecker C et al (1999) Neurocysticercosis. J Radiol 80:1623–1627
66. Raffin LS, Bacheschi LA, Machado LR et al (2001) Diffusion-weighted MR imaging of cystic lesions of neurocysticercosis: a preliminary study. Arq Neuropsiquiatr 59:839–842
67. Braga F, Rocha AJ, Gomes HR et al (2004) Noninvasive MR cisternography with fluid-attenuated inversion recovery and 100% supplemental O2 in the evaluation of neurocysticercosis. AJNR Am J Neuroradiol 25:295–297
68. Rodriguez Prado N, Llorente Pendas JL, Gomez Martinez JR et al (2004) Cerebellopontine angle and internal auditory canal lipomas: report of four cases and review of the literature. Acta Otorrinolaringol Esp 55:126–130
69. Sade B, Mohr G, Dufour JJ (2005) Cerebellopontine angle lipoma presenting with hemifacial spasm: case report and review of the literature. J Otolaryngol 34:270–273
70. Shin JH, Byun BJ, Kim DW, Choi DL (2002) Neurenteric cyst in the cerebellopontine angle with xanthogranulomatous changes: serial MR findings with pathologic correlation. AJNR Am J Neuroradiol 23:663–665
71. Preece MT, Osborn AG, Chin SS, Smirniotopoulos JG (2006) Intracranial neurenteric cysts: imaging and pathology spectrum. AJNR Am J Neuroradiol 27:1211–1216
72. Chaynes P, Thorn-Kany M, Sol JC et al (1998) Imaging in neurenteric cysts of the posterior cranial fossa. Neuroradiology 40:374–376
73. Shakudo M, Inoue Y, Ohata K, Tanaka S (2001) Neurenteric cyst with alteration of signal intensity on follow-up MR images. AJNR Am J Neuroradiol 22:496–498
74. Bonneville F, Barrali E, Cattin F et al (1999) What is your diagnosis? Cholesterol granuloma or cholesterol cyst. J Neuroradiol 26:147–149
75. Warakaulle DR, Anslow P (2003) Differential diagnosis of intracranial lesions with high signal on T1 or low signal on T2-weighted MRI. Clin Radiol 58:922–933